4.

Buckling strength of FML profiles of 'classic' versus thin-ply design

4.1. Introduction

The past few decades have seen the introduction of fiber metal laminates (FMLs), especially GLARE, into primary structure applications such as the fuselage of the largest civil transport aircraft in current production: the Airbus A380. GLARE material properties, as well as FMLs in general, exhibit partly metallic and partly composite behaviour. The hybrid nature of FML has several advantages when compared with monolithic aluminium application to fuselage skins, i.e. lower density and crack arresting capability of the fiber layers in presence of a fatigue cracks, which are a major concern in the design of monolithic aluminium [4.23]. The possibility to tailor the material to meet specific structural or mechanical requirements, by appropriate orientation of the fibers layers, is especially important. These features allow to some extent the concerns about `flying with undetectable fatigue damage´, which influences inspection intervals and the economics of airframe maintenance [4.2].

The benefits of fiber metal laminates result from their architecture, which contain layers of unidirectional glass fibre-reinforced material sandwiched between thin aluminium sheets. Various properties can be achieved according to the different grades of GLARE developed for specific applications in aircraft members [4.22]. A common lay up for thin sheets is the 3/2 layup with either 0.3 mm or 0.4 mm individual aluminium sheet thickness. However, the merits for time dependent properties of FML applications and weight saving effects lead also to a thin-walled design of aircraft structures and to higher stress acceptance. That provides a possibility that thin-walled sections may undergo different modes of buckling. Therefore, particularly for slender and thin-walled elements, the stability phenomenon becomes one of the most important factors that needs to be investigated for safety reasons [4.21].

From the maintenance reasons the main research of FML structures was focused on fatigue properties and crack propagation. Based upon this research, it was concluded that the main advantages of FMLs over monolithic aluminium alloys are the increased fatigue and corrosion resistance [4.22]. Despite

previously introduced aramid fibres, soon replaced by glass fibres, also other constituents were considered, such as carbon/epoxy composite, polyamide, ß titanium or stainless steel - to be mentioned. Although, the dominant material still consist of laminated GFRP with aluminium alloys [4.1, 4.15]. In aerospace and aviation introduction of fiber metal laminate elements - among them FML skin panels, revealed that at some locations in a stiffened fuselage skin panel, monolithic aluminium stringers lead to insufficient interaction. The higher elastic modulus of the aluminium stringers would attract more load from the skin panels, which creates fatigue problems in the stringers. Therefore some FML stringers have been developed [4.7]. The solution mostly adopted in manufacturing allow to first lay-up the complete laminate stack and pre-form it wet before curing. The stiffener is either bonded to the skin with a polymer adhesive containing a carrier, or by a fibre reinforced polymer with reduced FVF. It can carry different type of loads - out of plane as well as in-plane compression. Thus, the objective of current chapter is the buckling analysis of thin-walled profiles of open cross-section made of FML type materials. This area of research devoted to the fibre reinforced metal laminates is relatively not fully covered and the number of publications is limited [4.14].

4.2. Subject of research

Under experimental and numerical considerations were thin-walled fibre metal laminate profiles of Z-shape and channel cross sections. Both types of investigated short columns have the same overall dimensions, i.e. the width of the web was equal to 80 mm, flange to 40 mm, with a profile length ca. 300 mm. A corner radius (R) of the web and flange junction bent was approximately equal to 1.75 mm (Fig. 4.1 a, b).
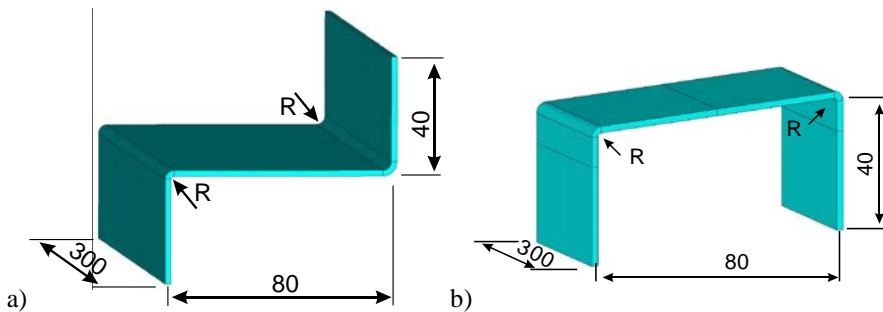

Fig. 4.1. Overall dimensions of Z-shape a) and channel section b)

Laminated FML columns were completed to appropriate stacking in a wet form and next cured with the autoclave technique in the Department of Materials

Engineering at the Lublin University of Technology [4.5]. Some specific information and manufacturing procedures applied for manufacturing of FML specimens are discussed also in [4.14]. All manufactured specimens were of 3/2 type FML, thus, 7-layered hybrid laminate of alternating plies of aluminium and fibre-reinforced composite. Applied aluminium was a 2024 T3 alloy with the thickness of a single layer equal to 0.3 mm, whereas for composite plies it was glass-epoxy unidirectional fibre-reinforced pre-preg TVR 380 M12 26% R-glass. The nominal volume fraction of the fibre equals 60% and the thickness of a single pre-preg layer after curing was equal to 0.25 mm. Then according to FML specification the 3/2 stacking indicates '3' aluminium layers where '2' refers to two embedded composite layers between aluminium sheets. In tested models and specimens particular GFRP layer was doubled with few fiber orientation chosen (Fig. 4.2). However, only symmetrical lay-ups with respect to column wall mid-plane were investigated.
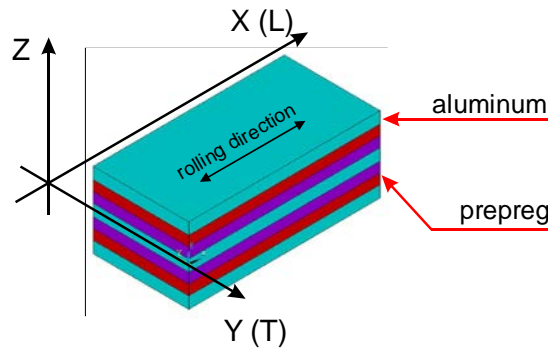

Fig. 4.2. 3/2 FML layup configuration

Table 4.1. Considered stacking sequences

FML No.	Lay-up
1	Al/0/90/Al/90/0/Al
2	Al/90/0/Al/0/90/Al
3	Al/45/0/Al/0/45/Al
4	Al/0/45/Al/45/0/Al
5	Al/0/0/Al/0/0/Al
6	Al/25/0/Al/0/25/Al
7	Al/0/25/Al/25/0/Al
8	Al/*Al*/*Al*/Al/*Al*/*Al*/Al
9	Al/*Iso*/*Iso*/Al/*Iso*/*Iso*/Al
10	Al/45/-45/Al/-45/45/Al

Depending on fibres alignment few various stacking sequences of FML were considered and compared in buckling and post-buckling analysis. They are presented in Table 4.1 but only first seven lay-ups were manufactured and tested in the laboratory. Some among chosen sequences are standard GLARE grades, as: FML 1 - GLARE 3; FML 5 - GLARE 2A; FML 10 - GLARE 6A while others (FML 6 and 7), containing shallow angle sub-laminates were chosen for comparison as possible future designs; they contain designs matching current trends in non-crimp fabric development. FML 8 represents a monolithic aluminium profile, providing a datum configuration against which all other designs can be compared. An alternative data is represented by FML 9, containing composite layers with fully isotropic properties [4.26].

Mechanical properties for aluminium are given in Table 4.2, and those of glass-epoxy pre-preg from TVR Hexcel composites are given in Table 4.3. Due to discrepancies observed during the buckling experiments [4.14], these properties were measured in laboratory tests [4.11], leading better agreement between experiment, analytical and numerical results than was achieved when using the data provided by the material supplier.

Table 4.2. Material properties for aluminium

Material properties		Aluminium 2024-T3
Compressive moduli	E_1	77.00 GPa
(very small orthotropy for yield limit)	E_2	77.00 GPa
Shear modulus	G_{12}	28.95 GPa
Poison's ratio	ν_{12}	0.33

Table 4.3. Material properties for R-Glass/Epoxy and Carbon/Epoxy composite

Material properties		R-Glass/Epoxy (Hexcel[TM])	Carbon/Epoxy 120EP-513/CF
Compressive moduli	E_1	53.90 GPa	136.1 GPa
	E_2	14.92 GPa	7.01 GPa
Shear modulus	G_{12}	5.49 GPa	4.661 GPa
Poison's ratio	ν_{12}	0.28	0.274

4.3. Buckling problem

The aforementioned short FML columns/profiles, chosen for investigation, were generally examined with application of three methods. These were - analytical numerical method based on Koiter's asymptotic theory of conservative systems [4.12], the finite element method [4.4] and laboratory experiment

performed in a universal testing machine [4.14]. For all three approaches it was assumed that the loaded edges of axially compressed columns are simply supported. This rather mathematical statement is relatively easy to fulfil in analytical solution. In numerical approach for model discretized with shell finite elements (Fig. 4.3b), it can be achieved by properly selected constrains at loaded edges of considered profiles. However, it is rather difficult to achieve appropriate conditions equivalent to this mathematical formulation in buckling experimental tests [4.13, 4.19]. Nevertheless, in current study we managed to design loading platens which reproduced idealized analytical and numerical boundary conditions in sufficient way. It was a shallow groove of flat bottom, with chamfered edges, milled in both platens, with a small clearance left for profile wall thickness. Additionally, the thickness of both upper and lower loading grids ensured the uniform compression of the profile, gave also the uniform displacement of loaded edges and axial adjustment of compression force (Fig. 4.3a).
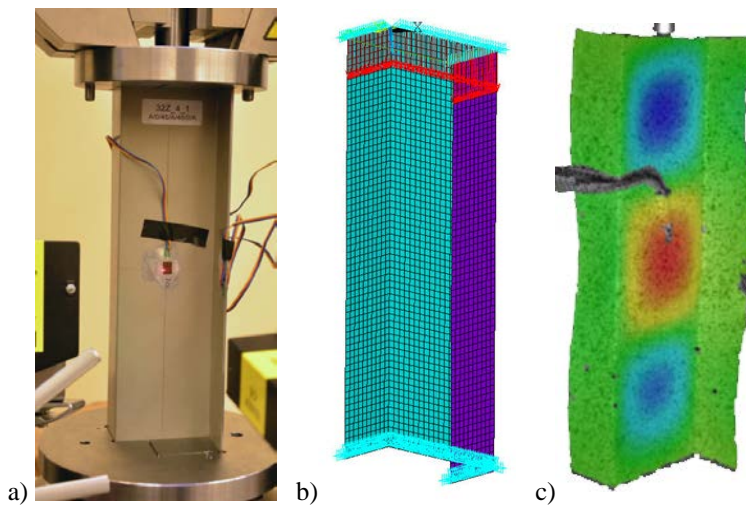

a) b) c)

Fig. 4.3. FML columns: a) laboratory stand, b) FEM model, c) DIC buckling mode

The applied measurement techniques during buckling experiments and methods of data processing one can find in [4.13, 4.14, 4.16]. In subsequent text only final results will be discussed. A very spectacular method occurred the Digital Image Correlation technique which is 3D non-contact optical measuring system of surface deformations (Fig. 4.3c). Its imaging of buckling modes confirmed analytical and numerical predictions and the compatibility of all investigations.

4.4. Buckling load comparison

As an example, for discussion, some results obtained for channel section will be compared. Those for Z-shape profile were presented and thoroughly discussed in [4.4, 4.13, 4.14]. In Table 4.4 buckling force values determined in experiment, FEM and analytical-numerical method are summarized. Not all manufactured FML specimens were included in laboratory test program thus 'nd' description visible in few rows. Also the last three lay-ups were not tested and introduced for further discussion.

Among results in Table 4.4 a good agreement can be observed between buckling loads determined in laboratory tests and finite element computations. Buckling force values for particular GFRP layer sequences of FML profiles calculated with analytical-numerical method are lower due to neglecting the corner radius at the web and flange joints. It lowers a stiffness of entire column therefore also its buckling force. When compared to experiment the differences of buckling force values rise up to 11%, whereas for the first two methods do not exceed 4%.

Table 4.4. Buckling loads of FML channel section columns

FML No.	Lay-up	Buckling force		
		exp	FEM	ANM
		[kN]	[kN]	[kN]
1	Al/0/90/Al/90/0/Al	31.434	30.189	28.568
2	Al/90/0/Al/0/90/Al	nd	29.871	28.408
3	Al/45/0/Al/0/45/Al	32.634	31.399	29.876
4	Al/0/45/Al/45/0/Al	nd	30.588	29.015
5	Al/0/0/Al/0/0/Al	29.836	30.310	28.630
6	Al/25/0/Al/0/25/Al	nd	30.745	29.334
7	Al/0/25/Al/25/0/Al	29.856	30.977	28.859
8	Al/*Al/Al*/Al/*Al/Al*/Al	nd	40.472	38.510
9	AL/*Iso/Iso*/AL/*Iso/Iso*/Al	nd	30.805	31.380
10	Al/45/-45/Al/-45/45/Al	nd	31.752	30.208

If we compare the buckling force value of a particular FML profile to that of a fully aluminium section, there is a noticeable reduction of buckling load. Among the other sections considered, this effect is especially pronounced for the Al/90/0/Al/0/90/Al cross-ply stacking sequence, where this reduction is as high as 26%, compared to approximately 22% for the Al/45/-45/Al/-45/45/Al angle-ply FML profile. The source of this degradation is of course the noticeable difference between Young's moduli of aluminium and glass-epoxy pre-preg but

among different FML stacking sequences it is the off-axis material alignment which in some cases leads to bending-twisting coupling. The sequence in which the layers are stacked can be tailored in order to control stiffness coupling. However, this effect has yet to be thoroughly quantified against practical designs. In the case of the buckling problem, the arrangement of plies must be 'tailored' with respect to their distance from the laminate mid-plane, since this influences the bending stiffness matrix, **D**, and in turn the buckling response. The literature describes strategies for identifying coupled laminate configurations with generic angle- and cross-ply combinations, which approximate fully isotropic behaviour [4.18, 4.26].

Although there is a perceived disadvantage due to lower buckling load for profiles made of hybrid FML material, this is outweighed by a spectacular mass reduction, which for the thin-walled columns investigated, reaches approximately 15%; a weight reduction which is an important factor in material selection for commercial aircraft applications [4.22].

4.5. Coupling effect

The laminate constitutive equations, i.e. the relationship of the in-plane forces $\{N\}$ and moments $\{M\}$ to reference strain $\{\varepsilon\}$ and curvature $\{\kappa\}$ can be combined into one brief, well-known matrix equation [4.10, 4.17]

$$\left\{ \begin{array}{c} \{N\} \\ \{M\} \end{array} \right\} = \left[\begin{array}{cc} [A] & [B] \\ [B] & [D] \end{array} \right] \left\{ \begin{array}{c} \{\varepsilon^{(0)}\} \\ \{\kappa\} \end{array} \right\} \tag{4.1}$$

The equations (4.1) are expressed in terms of three laminate stiffness matrices, extensional $[A]$, coupling $[B]$, and bending $[D]$, which are functions of the geometry, material properties and stacking sequence of the individual plies [4.10]. The coupling behaviour is dependent on the form of the elements in each of these three stiffness matrices. Balanced and symmetric stacking sequences - as assumed in the case of the FML columns considered, generally possess Bending-Twisting coupling; often referred to as bending anisotropy in the literature. There are some efforts to remove this disadvantage regardless the position of reference plane which can be shifted, such as in the corner between the web and flange of a Channel-section or Z-section [4.9].

These coupling effects are described in detail by the Engineering Sciences Data Unit (ESDU) [4.8]. A Bending-Twisting coupled laminate, with the designation **A**S**B**0**D**F, signifies that the elements of the extensional stiffness matrix $[A_S]$ are Specially orthotropic or Simple in nature, i.e. uncoupled, since

$$A_{16} = A_{26} = 0 \tag{4.2}$$

the bending-extension coupling matrix $[B_0]$ is null and all elements of the bending stiffness matrix $[D_F]$ are Finite, i.e. $D_{16}, D_{26} \neq 0$. The subscripts used can be further extended to indicate extensional isotropy, where $\mathbf{A_I}$ replaces $\mathbf{A_S}$ when

$$A_{16} = A_{26} = 0 \tag{4.3}$$

and

$$A_{66} = (A_{11} - A_{22})/2 \tag{4.4}$$

Additionally, bending isotropy, can be indicated by replacing $\mathbf{D_S}$ with $\mathbf{D_I}$, when

$$D_{ij} = A_{ij} H^2/12 \tag{4.5}$$

where *H* is a total laminate thickness corresponding to the total number of plies, *n*, of thickness *t* [4.26].

Tsai and Pagano introduced the very useful concept of the laminate invariants U_i [4.10, 4.20], which are calculated from the reduced stiffness matrix terms Q_{ij}

$$
\begin{aligned}
U_1 &= (3Q_{11} + 3Q_{22} + 2Q_{12} + 4Q_{66})/8 \\
U_2 &= (Q_{11} - Q_{22})/2 \\
U_3 &= (Q_{11} + Q_{22} - 2Q_{12} - 4Q_{66})/8 \\
U_4 &= (Q_{11} + Q_{22} + 6Q_{12} - 4Q_{66})/8 \\
U_5 &= (Q_{11} + Q_{22} - 2Q_{12} + 4Q_{66})/8
\end{aligned} \tag{4.6}
$$

and the reduced stiffness terms are calculated from the material properties [4.20]

$$
\begin{aligned}
Q_{11} &= E_1/(1 - v_{12}v_{21}) \\
Q_{12} &= v_{12} E_2/(1 - v_{12}v_{21}) \\
Q_{22} &= E_2/(1 - v_{12}v_{21}) \\
Q_{66} &= G_{12}
\end{aligned} \tag{4.7}
$$

Then the stiffness properties for the Equivalent Fully Isotropic Laminate can be obtained from the laminate invariants of Eqs. (4.6), expressed in terms of their isotropic material counterparts, with the assumption that $E_1 = E_2$, $v_{12} = v_{21}$, etc.

$$E_{Iso} = 2(1 + v_{Iso})G_{Iso} = U_1(1 - v_{Iso}^2) \tag{4.8}$$

with $\nu_{Iso} = U_4/U_1$ and $G_{Iso} = U_5$. The Young's modulus E_{Iso}, and Poisson ratio ν_{Iso}, and shear modulus G_{Iso}, are the equivalent isotropic material properties of a composite laminate of thickness, H, consisting of the total number of plies, n, of uniform thickness t. Thus, the equivalent isotropic stiffness properties for laminates with any number of plies can be expressed as follows

$$A_{Iso} = A_{11} = A_{22} = E_{Iso}H/\left(1 - \nu_{Iso}^{2}\right) = U_1 H$$
$$A_{12} = \nu_{Iso}A_{11} \tag{4.9}$$
$$A_{66} = U_5 H$$

The bending stiffness elements follow from Eq. (4.5) as

$$D_{Iso} = E_{Iso}H^{3}\left(1 - \nu_{Iso}^{2}\right)/12 = U_1 H^{3}/12 \tag{4.10}$$

Although the most commonly adopted method for achieving fully uncoupled laminates is the ubiquitous balanced and symmetric lay-up, non-symmetric laminate configurations are now known to dominate the design space of *Simple* (uncoupled), as well as *Bending-Twisting* coupled laminates [4.25, 4.28]. Therefore some optimization technique are used for free form ply angle orientation and higher number of ply groupings [4.18].

Applying these formulae to the FML designs considered, one can obtained the equivalent bending stiffness D_{Iso} = 49391 N·mm for FML 8 (monolithic aluminium) of Table 4.1, whereas for FML 9, D_{Iso} = 39223 N·mm, for R-Glass/Epoxy (Hexcel[TM]) when H = 1.9 mm, used in the normalization of buckling load results.

For FML designs with Carbon/Epoxy 120EP-513/CF sub-laminates H = 1.86 mm, and FML 8 gives D_{Iso} = 46336 N·mm, whereas for FML 9 D_{Iso} = 41447 N·mm. In all FML designs, $D_{ij} \neq A_{ij}H^{2}/12$ due to the lamination of more than one material.

The reduction in bending stiffness below monolithic aluminium results in decreased buckling load value (Table 4.4). Taking as a reference the buckling load of aluminium channel profile (FML 8) to normalize the buckling results for other sequences and additionally for a rectangular plate matching the aspect ratio a/b = 3.75, corresponding to the same aspect ratio as the web of the channel section, this effect can be directly assessed in Table 4.5. The buckling load is approximately 25% below that of the monolithic aluminium profile, and a similar drop is observed for the comparison between the rectangular plate results.

A solid aluminium section profile and/or flat plate made from GFRP material designed as an Equivalent Fully Isotropic Laminate possesses higher buckling strength than those made from standard GLARE 3 (or FML 1 in

Table 4.5), or GLARE 6A (or FML 10). The differences between the GLARE 3 and 6A are less than 5%.

Table 4.5. Buckling comparisons between channel section buckling load and plate buckling factor, with matching web and plate aspect ratio ($a/b = 3.75$) for standard GFRP material or GLARE. Overall FML thickness $H = 1.9$ mm

FML	Buckling Load - Channel [kN]*	Relative Buckling strength	Buckling factor - Plate (k_x)	Relative Buckling strength
1	28.258	-22.5%	3.03	-24.5%
5	28.346	-22.2%	3.04	-24.3%
8	36.439	0.0%	4.02	0.0%
10	29.818	-18.2%	3.14	-21.8%

It is obvious that replacing R-glass composite layers with carbon composite plies will give lower discrepancy in Young's moduli between both constituents and the equivalent bending stiffness differences will be less than for standard GLARE designs. The effect of such an exchange is visible in Table 4.6 where results are analogues to those from Table 4.5. The modified material properties are given in Table 4.3 [4.3, 4.6]. In first row, the notation 'AS60' represents an FML with a Quasi-Homogenous Orthotropic sub-laminate $[\pm45_2/-45_2/45_2/\pm45_2]$ with NORTH PLY material of areal weight 60 gsm and ply thickness $t = 0.02$ mm. The drop of a buckling force, when compared to monolithic aluminium channel or plate, is much lower than for R-glass composite. The FML with an isotropic sub-laminate is approximately 10% lower, whilst the orthotropic sub-laminates is as little as 4% lower. The improvement of buckling features is therefore pronounced.

Table 4.6. Buckling comparisons between Channel section buckling load and plate buckling factor, with matching web and plate aspect ratio ($a/b = 3.75$) for NORTH PLY CFRP material. Overall FML thickness $H = 1.86$ mm

FML	Buckling Load - Channel [kN]*	Relative Buckling strength	Buckling factor - Plate (k_x)	Relative Buckling strength
AS60	33.069	-3.3%	3.81	-5.2%
8	34.189	0.0%	4.02	0.0%
9	30.719	-10.1%	3.59	-10.6%
10	32.806	-4.0%	3.78	-5.9%

Differences in the relative bucking strength between the channel section and the simply supported plate demonstrate the weak influence that the flanges have on web buckling.
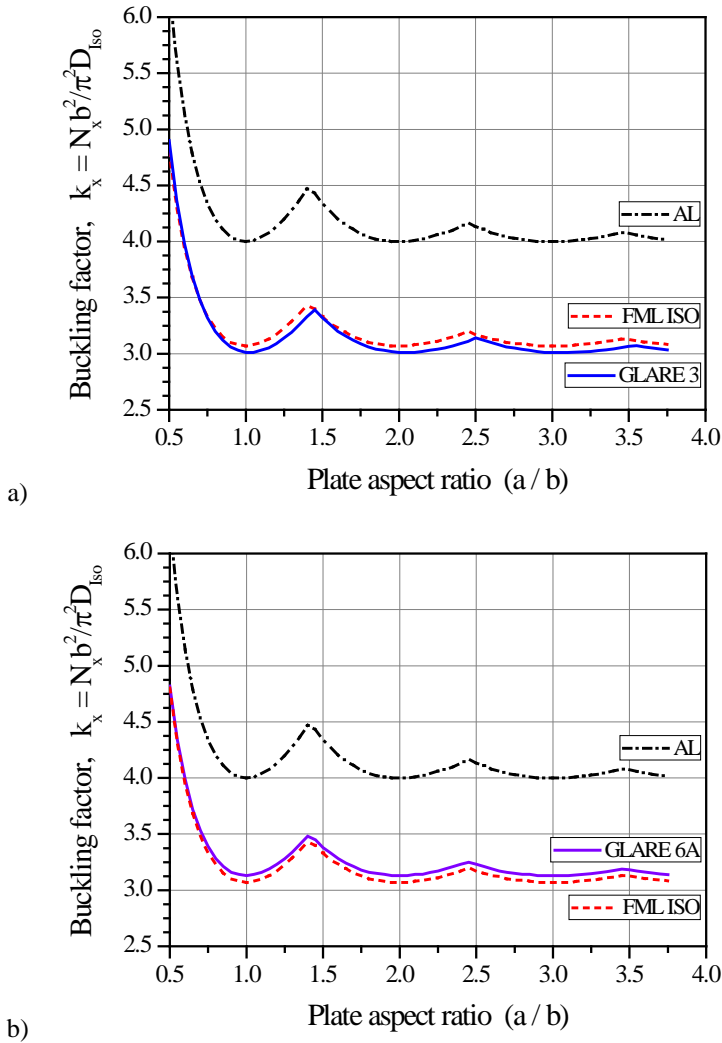

a)

b)

Fig. 4.4. Compression buckling factor curves for Standard FML designs with aluminium and R-Glass/Epoxy: (a) GLARE 3 [Al/0/90/Al/90/0/Al]$_T$ and (b) GLARE 6A [Al/45/-45/Al/-45/45/Al]$_T$

The relative difference between buckling loads for profiles made of different FML grades with carbon-epoxy layers looks similarly to the relationships observed in Fig. 4.4, but the distances between garland curves are bigger

(Fig. 4.5). It can be noticed that GLARE 6A (FML 10) has reducing buckling strength, i.e. 5.39%, 5.72% and 5.84% below the datum (Aluminium plate) for $a/b = 1$, 2, and 3 respectively. This effect is caused by Bending-Twisting coupling in the carbon/epoxy sub-laminate.
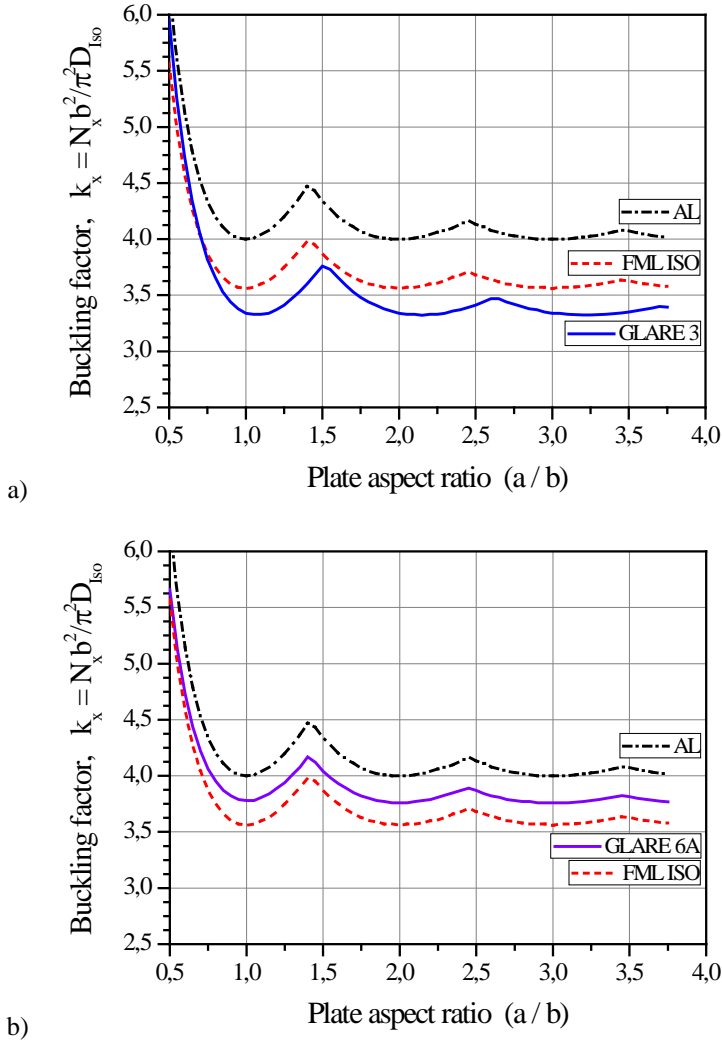

a)

b)

Fig. 4.5. Compression buckling factor curves for standard FML designs with aluminium and carbon/epoxy: a) GLARE 3 [Al/0/90/Al/90/0/Al]$_T$ and b) GLARE 6A [Al/45/-45/Al/-45/45/Al]$_T$. Al. and FML$_{ISO}$ represent a monolithic aluminium design and a standard FML design but with an isotropic carbon/epoxy sub-laminate

These results demonstrate that carbon/epoxy has the potential to substantially increase buckling strength in FML designs. However, FML designs with isotropic or tailored sub-laminates require thin ply material technology to achieve the required stacking sequence configurations yet remain within the thickness constraint of standard FML designs.

4.6. Thin-ply technique

During the last decade evident progress has been made in the development of composite laminates using thinner plies. When the areal weights of standard composite materials equals 300 gsm for thin-ply pre-pregs are commercially available down to as little as 30 gsm, with a corresponding thickness of 20 μm per single ply depending on the type of fibre. This generally increases the scope for laminate tailoring without affecting laminate thickness or weight.

The most important benefit of using thinner plies in a laminate design, for a constant laminate thickness, is the ability to use a larger number of ply orientations to achieve an optimal solution as the laminate design space is naturally extended. The second merit is that thin-ply composites may present some advantages due to positive size effects with respect to decreasing ply thickness. Although the use of thin-ply pre-pregs leads to increase in manufacturing cost, the damage resistance properties against matrix cracking and delamination significantly improve. Despite identical stiffness of thin-ply and standard laminates compared, the tensile strength of the laminate using the thin-ply pre-pregs is higher than that of the laminate using the standard pre-pregs [4.24]. Composite laminates manufactured from thin-ply pre-pregs are believed to have superior damage resistance properties compared to those from standard pre-pregs. They are less susceptible to matrix crack accumulation than the standard laminate and to propagation of free-edge delamination. These observations have been verified experimentally [4.24].

Some pseudo-ductile effects were observed in the response of unidirectional interlayer hybrid composite materials comprising R-glass and a variety of thin carbon pre-pregs [4.6]. The materials considered for this hybrid design and examined in set of experiments were standard thickness R-glass/epoxy pre-pregs supplied by Hexcel, thin S3-glass/epoxy from North Thin Ply Technology and various thin carbon/epoxy pre-pregs from SK Chemicals and North Thin Ply Technology. The epoxy resin systems used in the pre-pregs were the aerospace grade 913 (Hexcel), Thin-Preg 120 EPHTg-402 (North Thin Ply Technology) and K50 (SK chemicals). The developed material suitable for dominated tensile loads exhibit a 60 GPa initial modulus, up to 970 MPa pseudo-yield stress and 1.44% pseudo-ductile strain.
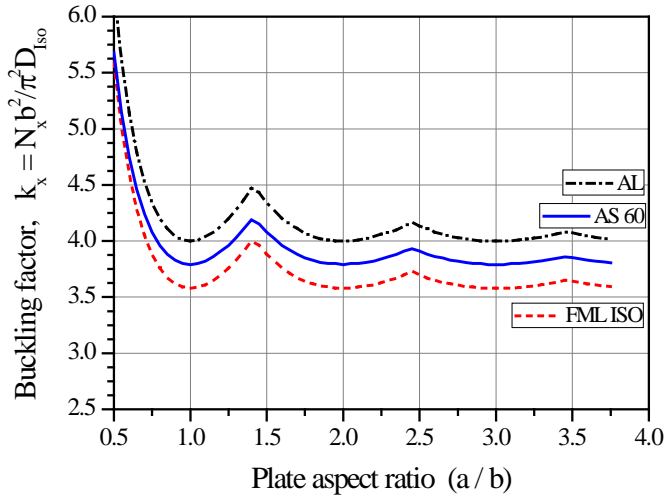
a)
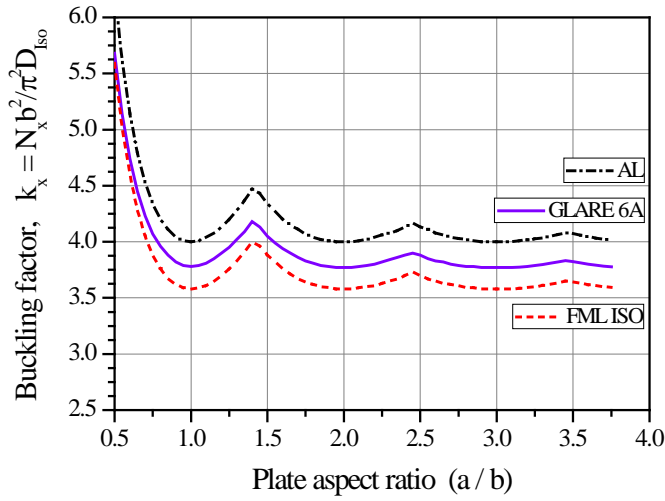
b)

Fig. 4.6. Compression buckling factor curves for NORTH PLY FML designs
with aluminium and Carbon/Epoxy (60gsm):
a) GLARE 3 [Al/$\pm45_2$/-45_2/45_2/$\pm45_2$/Al/$\pm45_2$/-45_2/45_2/$\pm45_2$/Al]$_T$
and b) GLARE 6A [Al/45_{12}/-45_{12}/Al/-45_{12}/45_{12}/Al]$_T$

In the available literature, which is not so abundant, there is some evidence
that thin-ply leads to a more uniform microstructure and improved on-axis
compressive strength, hence nearly no damage is observed in thin ply material
before failure. Some of these features result from the large number of sub-
laminate repetitions. These special material properties promise better

predictability of behaviour from laminates manufactured using thin-ply technology.

Returning our attention to the buckling strength of FML profiles, standard GLARE architectures with carbon-epoxy sub-laminates are replaced with thin plies of 60 gsm areal weight to create [Al/±45$_2$/-45$_2$/45$_2$/±45$_2$/Al/±45$_2$/-45$_2$/45$_2$/±45$_2$/Al]$_T$ and [Al/45$_{12}$/-45$_{12}$/Al/-45$_{12}$/45$_{12}$/Al]$_T$ stacking sequences with the same overall thickness. Buckling loads for these thin-ply FML designs are compared again with monolithic aluminium plates in Fig. 4.6. The relationships are similar to those for standard carbon/epoxy layers, with the major difference being the reduction of buckling load is significantly lower than for standard ply thickness.

Hybrid laminates have a strange mix of stiffness relationships. Sub-laminates may be designed to be fully isotropic with sufficient numbers of thin-ply layers, e.g. 24 layers: [-45/90/0/45/0/45/90/45/-45/0/-45/90/-45/90/45/90/0/-45/0/45/0/45/-45/90]$_T$, but the FMLs no longer satisfy Eq. (4.5). The hybridization renders the relationship proportional, rather than equal, i.e.: $D_{ij} \propto A_{ij} H^2/12$, even when the properties are isotropic in both extension and bending.

4.7. Lamination parameters for bending stiffness assessment of FML designs

Ply angle dependent lamination parameters may offer useful insight into the effects on buckling of different sub-laminate architectures, since they allow the bending stiffness terms to be expressed as linear variables within convenient bounds $\left(-1.0 \leq \xi_i \leq 1.0\right)$, which are readily presented in graphical form to aid the design process [4.26]. Four lamination parameters exist for each of the extension $\left(\xi_1 - \xi_4\right)$, coupling $\left(\xi_5 - \xi_8\right)$ and bending $\left(\xi_9 - \xi_{12}\right)$ stiffness matrices. For the buckling assessment of laminated composite plates, only those for bending stiffness are of importance, given that the coupling stiffnesses are assumed to be zero. Lamination parameters $\left(\xi_9 - \xi_{12}\right)$ for FML are related to the elements of the bending stiffness matrix as follows

$$
\begin{Bmatrix} D_{11} \\ D_{12} \\ D_{16} \\ D_{22} \\ D_{26} \\ D_{66} \end{Bmatrix} = \frac{\zeta^{Al}}{\zeta} \frac{H^3}{12}
\begin{bmatrix}
1 & \xi_9^{Al} & \xi_{10}^{Al} & 0 & 0 \\
0 & 0 & -\xi_{10}^{Al} & 1 & 0 \\
0 & \xi_{11}^{Al}/2 & \xi_{12}^{Al} & 0 & 0 \\
1 & -\xi_9^{Al} & \xi_{10}^{Al} & 0 & 0 \\
0 & \xi_{11}^{Al}/2 & -\xi_{12}^{Al} & 0 & 0 \\
0 & 0 & -\xi_{10}^{Al} & 0 & 1
\end{bmatrix}
\begin{Bmatrix} U_1^{Al} \\ U_2^{Al} \\ U_3^{Al} \\ U_4^{Al} \\ U_5^{Al} \end{Bmatrix} +
$$

$$
\frac{\zeta^{FRP}}{\zeta} \frac{H^3}{12}
\begin{bmatrix}
1 & \xi_9^{FRP} & \xi_{10}^{FRP} & 0 & 0 \\
0 & 0 & -\xi_{10}^{FRP} & 1 & 0 \\
0 & \xi_{11}^{FRP}/2 & \xi_{12}^{FRP} & 0 & 0 \\
1 & -\xi_9^{FRP} & \xi_{10}^{FRP} & 0 & 0 \\
0 & \xi_{11}^{FRP}/2 & -\xi_{12}^{FRP} & 0 & 0 \\
0 & 0 & -\xi_{10}^{FRP} & 0 & 1
\end{bmatrix}
\begin{Bmatrix} U_1^{FRP} \\ U_2^{FRP} \\ U_3^{FRP} \\ U_4^{FRP} \\ U_5^{FRP} \end{Bmatrix}
$$

(4.11)

where ζ^{Al} and ζ^{FRP} are non-dimensional bending stiffness parameters representing the contribution of the Aluminium (*Al*) and Fibre Reinforced Plastic (*FRP*) sub-laminates, with $\zeta = \zeta^{Al} + \zeta^{FRP}$. Assuming uniform ply thickness throughout, $\zeta = n^3$, where *n* in the number of plies in the laminate, or, in this case, to satisfy non-uniform ply thickness between *Al* (0.3 mm) and *FRP* (0.25 mm) layers, a suitable fraction (0.05mm) that permits the build-up of (6 or 5) contiguous plies to achieve the required thicknesses. The laminate invariants U_i are given in Eq. (4.6), noting that these are different for Carbon/epoxy or Glass/epoxy. Hence the lamination parameters for hybrid designs cannot be assessed in the same way as standard fibre/epoxy material designs. Nevertheless, some degree of assessment is possible through inference; based on standard fibre/epoxy laminate properties, since the Aluminium sub-laminate will always be represented by the lamination parameter point for an isotropic laminate, if the layers are symmetrically placed about the laminate mid-plane. Standard ply orientations (±45°, 0° and 90°) have been chosen specifically because they have most relevance to current design practice; this strategy also reduces the lamination parameter data to a 3-dimensional set, since the particularly choice of angle ply, $\pm\theta = \pm 45^o$, then renders $\xi_{12} = 0$. The isotropic laminate corresponds to the coordinate $(\xi_9, \xi_{10}, \xi_{11}) = (0.0, 0.0, 0.0)$ in the lamination parameter design space.

GLARE 6A contains an angle-ply sub-laminate, which corresponds to the lamination parameter coordinate (0.0, -1.0, 0.553). The bending stiffness contributions of the ζ^{Al} and ζ^{FRP} are 68% and 32% respectively.

The bending stiffness contributions are dependent on non-dimensional parameters relating to the geometric distribution of each sub-laminate, and are defined as

$$\zeta_{+45}^{FRP} = 4\sum\nolimits_{\theta=+45}\left(z_k^3 - z_{k-1}^3\right)/12\,, \;\; \zeta_{-45}^{FRP} = 4\sum\nolimits_{\theta=-45}\left(z_k^3 - z_{k-1}^3\right)/12\,,$$

$$\zeta_0^{FRP} = 4\sum\nolimits_{\theta=0}\left(z_k^3 - z_{k-1}^3\right)/12\,, \;\; \zeta_{90}^{FRP} = 4\sum\nolimits_{\theta=90}\left(z_k^3 - z_{k-1}^3\right)/12 \qquad (4.12)$$

where $\zeta^{FRP} = \zeta_{+45}^{FRP} + \zeta_{-45}^{FRP} + \zeta_0^{FRP} + \zeta_{90}^{FRP}$

Lamination parameters represent an angle ply dependent form of these non-dimensional parameters

$$\xi_9^{FRP} =$$
$$\left\{\zeta_{+45}^{FRP}\cos(2\times45°)+\zeta_{-45}^{FRP}\cos(2\times-45°)+\zeta_0^{FRP}\cos(2\times0°)+\zeta_{90}^{FRP}\cos(2\times90°)\right\}/\zeta^{FRP}$$

$$\xi_{10}^{FRP} =$$
$$\left\{\zeta_{+45}^{FRP}\cos(4\times45°)+\zeta_{-45}^{FRP}\cos(4\times-45°)+\zeta_0^{FRP}\cos(4\times0°)+\zeta_{90}^{FRP}\cos(4\times90°)\right\}/\zeta^{FRP}$$

$$\xi_{11}^{FRP} =$$
$$\left\{\zeta_{+45}^{FRP}\sin(2\times45°)+\zeta_{-45}^{FRP}\sin(2\times-45°)+\zeta_0^{FRP}\sin(2\times0°)+\zeta_{90}^{FRP}\sin(2\times90°)\right\}/\zeta^{FRP}$$

$$(4.13)$$

By contrast, for isotropic layers (*Al*),

$$\zeta^{Al} = \zeta_{+45}^{Al} = \zeta_{-45}^{Al} = \zeta_0^{Al} = \zeta_{90}^{Al} \qquad (4.14)$$

and given that *Al* can be considered as an *FRP* material with an infinite number of equally spaced fibre orientations, each with equal bending stiffness contribution,

$$\xi_9^{Al} \cong \zeta^{Al}\sum\nolimits_{i=1}^{\infty}\cos(2\theta_{i\pi/\infty}) = 0$$
$$\xi_{10}^{Al} \cong \zeta^{Al}\sum\nolimits_{i=1}^{\infty}\cos(4\theta_{i\pi/\infty}) = 0 \qquad (4.15)$$
$$\xi_{11}^{Al} \cong \zeta^{Al}\sum\nolimits_{i=1}^{\infty}\sin(2\theta_{i\pi/\infty}) = 0$$

or, as in this case equal numbers of fibres in each of the four standard fibre orientations. Additionally, the laminate invariants U_i of Eq. (4.6) for Aluminium lead to $U_2 = U_3 = 0$. These simplifying effects reduce Eqn. (4.11) to the following form

$$
\begin{Bmatrix} D_{11} \\ D_{12} \\ D_{16} \\ D_{22} \\ D_{26} \\ D_{66} \end{Bmatrix} = \frac{\zeta^{Al}}{\zeta} \frac{H^3}{12} \begin{Bmatrix} U_1^{Al} \\ U_4^{Al} \\ 0 \\ U_1^{Al} \\ 0 \\ U_5^{Al} \end{Bmatrix} + \frac{\zeta^{FRP}}{\zeta} \frac{H^3}{12} \begin{bmatrix} 1 & \xi_9^{FRP} & \xi_{10}^{FRP} & 0 & 0 \\ 0 & 0 & -\xi_{10}^{FRP} & 1 & 0 \\ 0 & \xi_{11}^{FRP}/2 & 0 & 0 & 0 \\ 1 & -\xi_9^{FRP} & \xi_{10}^{FRP} & 0 & 0 \\ 0 & \xi_{11}^{FRP}/2 & 0 & 0 & 0 \\ 0 & 0 & -\xi_{10}^{FRP} & 0 & 1 \end{bmatrix} \begin{Bmatrix} U_1^{FRP} \\ U_2^{FRP} \\ U_3^{FRP} \\ U_4^{FRP} \\ U_5^{FRP} \end{Bmatrix} \quad (4.16)
$$

and for GLARE 6A, the lamination parameter for the *FRP* sub-laminate is $\left(\xi_9, \xi_{10}, \xi_{11} \right) = \left(0.0, -1.0, 0.553 \right)$. The D_{ij} for the two sub-laminates, and the resulting FML, are given in Table 4.7.

Table 4.7. Comparison of relative bending stiffness between *GFRP* and *Al* sub-laminates for GLARE 6A

	D_{11}	D_{12}	D_{16}	D_{22}	D_{26}	D_{66}
FRP	4508	2523	982	4508	982	2754
Al	33765	11142	0	33765	0	11311
FML	38273	13665	982	38273	982	14065

4.8. Comparison with buckling results obtained from Carbon/Epoxy composite materials

For optimum design subject to buckling and/or strength constraints, ply angle dependent lamination parameters are often preferred, since these allow the stiffness terms to be expressed as linear variables within convenient bounds $\left(-1.0 \le \xi_i \le 1.0 \right)$. However, the optimized lamination parameters must then be matched to a corresponding laminate configuration within the feasible region. This inverse problem is often challenging, but is aided by graphical representations of the lamination parameter design spaces in which lamination parameter coordinates can be plotted. Buckling contour mapping can also be applied to these lamination design spaces, as illustrated in Fig. 4.7; here representing compression loaded infinitely long plates with simply supported edges.

Figure 4.7a indicates the feasible region of the 3-dimensional lamination parameter design space together with 3 cross-sections, taken on planes at $\xi_{11} = 0$, 0.5 and 0.6 to illustrate the variation in the buckling factor contours with increasing *Bending-Twisting* coupling.

a)

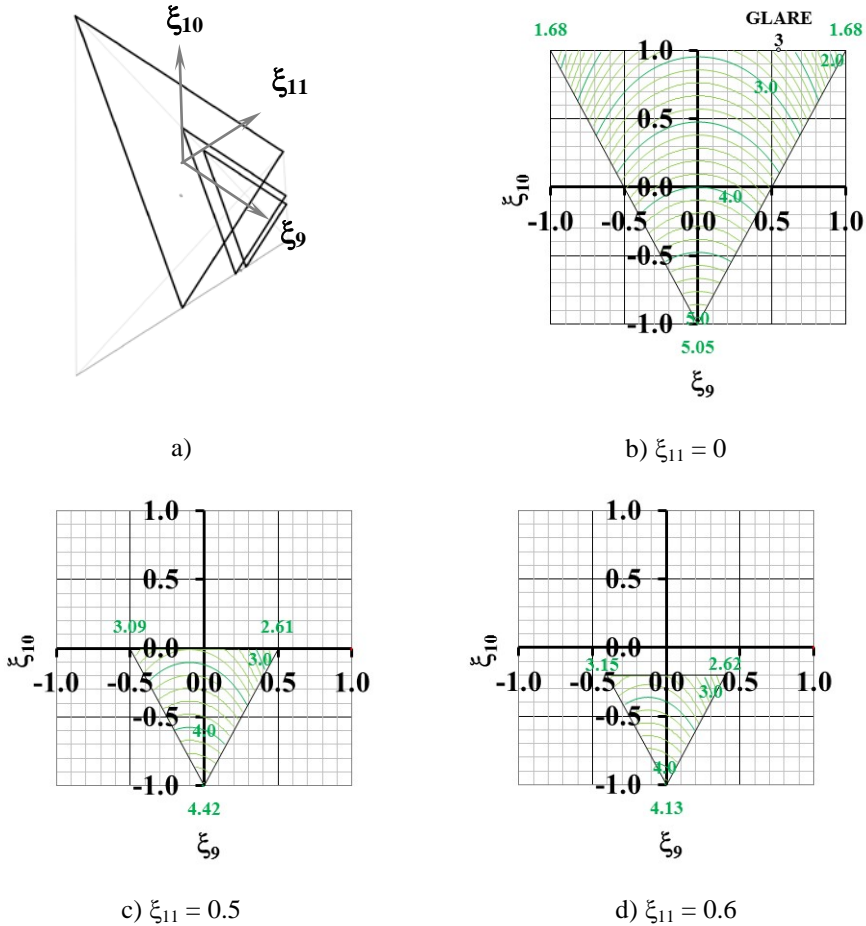b) $\xi_{11} = 0$

c) $\xi_{11} = 0.5$

d) $\xi_{11} = 0.6$

Fig. 4.7. The 3-dimensional lamination parameter design space illustrating a) cross-sectional planes onto which compression buckling contours ($k_{x,\infty}$) are mapped for infinitely long plates with simply supported edges, at
b) $\xi_{11} = 0.0$ on which the *Al* sub-laminate is located, c) $\xi_{11} = 0.5$ and
d) $\xi_{11} = 0.4$, between which the *FRP* sub-laminate corresponding to GLARE 6A is located, i.e. (ξ_9, ξ_{10}, ξ_{11}) = (0, -1, 0.553)

Cross-ply laminates, which are commonly adopted as sub-laminates in FML design (e.g. GLARE 3) can be plotted in Fig. 4.7b. Note that whilst these have equal number of 0 and 90° plies, the bending contributions are not equal due to the different interface distances about the laminate mid-plane. By contrast, balanced plain weave sub-laminates would possess equal bending stiffness contributions, with lamination parameter co-ordinate $\left(\xi_9, \xi_{10} = 0, 1\right)$. The

isotropic laminate with equal bending stiffness contributions from 0, 90, 45 and -45° plies corresponds to $(\xi_9, \xi_{10} = 0, 0)$ and possess the classical buckling load factor $k_{x,\infty} = 4.0$. Angle-ply sub-laminates with equal bending stiffness contributions from the +45 and -45° plies correspond to co-ordinate $(\xi_9, \xi_{10} = 0, -1)$, with buckling load factor $k_{x,\infty} = 5.05$.

Note that buckling loads are reduced whenever *Bending-Twisting* coupling is present, as is often the case in symmetric designs containing angle ply sub-laminates (e.g. GLARE 6A or 6B); the magnitude of the reduction increases with increasing *Bending-Twisting* coupling, in proportion to the corresponding lamination parameter $(\xi_{11} \geq 0)$. This is of course dependent on the volume fraction and relative position from the laminate mid-plane of each of the two material phases, hence the influence of *Bending-Twisting* coupling in FML is substantially reduced.

By contrast, *FRP* material is significantly affected by the presence of *Bending-Twisting* coupling. This is illustrated in the cross-sectional planes of Figs. 4.7c and 4.7d, which bound the *FRP* sub-laminate $(0.5 \leq \xi_{11} \leq 0.6)$ contained within GLARE 6A. This sub-laminate clearly has a significantly lower compression buckling strength $(4.13 < k_{x,\infty} < 4.42)$ than the angle-ply laminate ($k_{x,\infty} = 5.05$) in which the *Bending-Twisting* coupling has been eliminated through laminate tailoring.

These results demonstrate that the comparatively higher compression buckling strength of an angle-ply *FRP* sub-laminate does little to influence the buckling strength of the FML, even if the presence of *Bending-Twisting* coupling is ignored.

Glass/Epoxy sub-laminate provides a relatively insignificant contribution to bending stiffness and despite the increased stiffness of Carbon/Epoxy, including the elimination of the detrimental effects of *Bending-Twisting* coupling within the *FRP* sub-laminate, the high volume fraction of the metal layers in traditional FML severely limits the extent to which buckling strength can be improved by the use of laminate tailoring. In all cases, the FML resulted in a lower buckling factor than the monolithic Aluminium datum. However it should be noted that these comparisons did not consider specific buckling strength (k_x / ρ), taking into account the reduced density (ρ) of the hybrid material.

4.9. Conclusions

The aim of the work was a comparison of the application of 'classical' prepreg *FRP* layers versus 'thin-ply technology' designs, applied to FML plate structures. These included thin-walled Z-shape and channel cross-section profiles adopting a 3/2 FML lay-up design, made of 3 aluminium layers. Comparisons were made between composite sub-laminates with different materials, i.e. 'classical' glass-fiber prepreg (*GFRP*) and thin-ply carbon-fiber prepreg (*CFRP*). Different stacking sequences were also considered. Comparisons for the uni-axial compression buckling problem were obtained by various methods - among them an analytical-numerical method, a finite element method and an exemplary experimental investigations.

The hybridization of materials in multilayered structures for fatigue property improvement leads to an inevitable decrease in the buckling load capacity, but this effect is off-set to some extent by a measurable weight reduction. Multilayered *FRP* materials are very effective for meeting tailored structural property requirements through appropriate modification of the **A**, **B** and **D** matrices, which govern the laminate response. Controlling the bending stiffness [**D**] matrix through appropriate ply stacking sequence, material and ply thickness selection has been shown to give improvements in the compressive buckling load capacity for FML short columns of open cross-section. This was achieved through the introduction a thin-ply technology in the *FRP* sub-laminates to replace traditional *GFRP* or *CFRP* layers. Improvements in buckling strength of FML designs have been demonstrated through the use of lamination parameter design spaces onto which buckling factor contours can be mapped. This technique provides a very useful tool for assessment and prediction of new hybrid FML panel designs.

4.10. References

4.1 Alderliesten R., On the Development of Hybrid Material Concepts for Aircraft Structures, Recent Patents on Engineering, 3, 2009, pp. 25-38.

4.2 Alderliesten R.C., Designing for damage tolerance in aerospace: A hybrid material technology, Materials and Design, 66, 2015, pp. 421-428.

4.3 Amacher R., Cugnoni J., Botsis J., Sorensen L., Smith W., Dransfeld C., Thin ply composites: Experimental characterization and modelling of size-effects, Comp. Science and Technology, 101, 2014. pp. 121-132.

4.4 Banat D., Kolakowski Z., Mania R.J., Investigations of FML profile buckling and post-buckling behaviour under axial compression, Thin-Walled Structures, 107, 2016, pp. 335-344.

4.5 Bienias J., Fibre Metal Laminates - some aspects of manufacturing process, structure and selected properties, Compos. Theory Pract., 11, 2011, pp. 39-43.

4.6 Czél G., Jalalvand M., Wisnom M.R., Design and characterisation of advanced pseudo-ductile unidirectional thin-ply carbon/epoxy-glass/epoxy hybrid composites, Composite Structures, 143, 2016, pp. 362-370.

4.7 De Jong T.W., Kroon E., Sinke J., Formability, In: Vlot A., Gunnink J.W. (Eds.), Fibre Metal Laminates - an introduction, Kluwer Academic Publishers, Dordrecht, The Netherlands, 2001.

4.8 ESDU - Stiffnesses of laminated plates. Engineering sciences data unit, Item No. 94003; 1994.

4.9 Fletcher T.A., Butler R., Dodwell T.J., Erland S., Non-symmetric stacking sequences to aid manufacture, ECCM16 - 16TH European Conf. on Comp. Mat., Seville, Spain, 2014.

4.10 Jones R.M., Mechanics of Composite Materials, Taylor & Francis, London, 1999.

4.11 Kamocka M., Zglinicki M., Mania R.J., Multi-method approach for FML mechanical properties prediction, Composites Part B Eng., 91, 2016, pp. 135-143.

4.12 Kolakowski Z., Mania J.R., Semi-analytical method versus the FEM for analysis of the local post-buckling. Composite Structures, 97, 2013, pp. 99-106.

4.13 Mania R.J., Banat D., Modelling of boundary conditions in Fiber Metal Laminate buckling investigations, In: R.J. Mania (Ed.), Statics, Dyn. and Stab. of Struct., Buckling of Plate Struct. in Anal. and Numer. Exp. Investig., Vol. 4, Lodz University of Technology, Series of Monographs, 2016: pp. 49-66.

4.14 Mania R.J., Kolakowski Z., Bienias J., Jakubczak P., Majerski K., Comparative study of FML profiles buckling and postbuckling behaviour under axial loading, Composite Structures, 134, 2015, pp. 216-225.

4.15 Mathijsen D., Leading the way in thermoplastic composites, Reinforced Plastics, September 2015, in press, available online.

4.16 Paszkiewicz M., Kubiak T., Selected problems concerning determination of the buckling load of channel section beams and columns, Thin-Walled Structures, 93, 2015, pp. 112-121.

4.17   Reddy J.N., Mechanics of laminated composite plates and shells, theory and analysis, CRC Press, 2004.

4.18   Shamsudin M.H., York C.B., Mechanically coupled laminates with balanced plain weave, Composite Structures, Vol. 107, 2014, pp. 416-428.

4.19   Singer J., Arbocz J., Weller T., Buckling Experiments Experimental Methods in Buckling of Thin-Walled Structures. Willey, 1998.

4.20   Tsai S., Hahn H.T., Introduction to Composite Materials, Technomic Pub. Comp., 1980.

4.21   Verolme J.L., The initial buckling behavior of flat and curved fiber metal laminate panels. Delft University of Technology, Faculty of Aero. Eng, Report LR-785, 1995.

4.22   Vermeeren C. (ed.), Around GLARE, A new aircraft material in context. Kluwer Academic Publishers. 2004.

4.23   Vlot A. Gunnik J.W., Fiber Metal Laminates, An Introduction. Springer Science+Busines Media B.V., 2001.

4.24   Yokozeki T., Aoki Y., Ogasawara T. Experimental characterization of strength and damage resistance properties of thin-ply carbon fiber/toughened epoxy laminates, Composite Structures, 82, 2008, pp. 382-389.

4.25   York C.B., Characterization and ply mixing rules for non-symmetric forms of fully orthotropic laminates, 48th AIAA/ASME/ASCE/AHS/ASC Structures, Structural Dyn. and Mat. Conf., Honolulu, 2007, pp. 1-24

4.26   York C.B., Unified approach to the characterization of coupled composite laminates: benchmark configurations and special cases. Journal of Aerospace Engineering 2010;23:219-242.

4.27   York C.B., On Extension-Shearing coupled laminates. Composite Structures, 120, 2015, pp. 472-482.

4.28   York C.B., Influence of bending-twisting coupling on compression and shear buckling strength (Keynote), Proc. of Stability of Structures 14th Symposium, Zakopane, Poland, 2015, pp. 23-24.